

# Does host contact structure reduce pathogen diversity?

A. Nunes<sup>a\*</sup>, M. M. Telo da Gama<sup>a</sup> and M. G. M. Gomes<sup>b</sup>

<sup>a</sup>*Centro de Física Teórica e Computacional and Departamento de Física,  
Faculdade de Ciências da Universidade de Lisboa,*

*P-1649-003 Lisboa Codex, Portugal*

<sup>b</sup>*Instituto Gulbenkian de Ciência, Apartado 14, 2781-901 Oeiras, Portugal*

*\*Corresponding author: anunes@ptmat.fc.ul.pt*

## Abstract

We investigate the dynamics of a simple epidemiological model for the invasion by a pathogen strain of a population where another strain circulates. We assume that reinfection by the same strain is possible but occurs at a reduced rate due to acquired immunity. The rate of reinfection by a distinct strain is also reduced due to cross-immunity. Individual based simulations of this model on a 'small-world' network show that the host contact network structure significantly affects the outcome of such an invasion, and as a consequence will affect the patterns of pathogen evolution. In particular, host populations interacting through a 'small-world' network of contacts support lower prevalence of infection than well-mixed populations, and the region in parameter space for which an invading strain can become endemic and coexist with the circulating strain is smaller, reducing the potential to accommodate pathogen diversity. We discuss the underlying mechanisms for the reported effects, and we propose an effective mean-field model to account for the contact structure of the host population in 'small-world' networks.

## I. INTRODUCTION

Pathogens that diversify and evolve over relatively short time scales are associated with specific features of infectious disease epidemiology. Epidemics of acute respiratory infection occurring each winter in temperate climates are caused in general by influenza (Hay 2001) and respiratory syncytial viruses (Cane 2001). Rotaviruses (Iturriza-Gómara 2004) are the single most common cause of acute infantile gastroenteritis throughout the world. These viruses undergo antigenic drift and both influenza A and rotaviruses undergo major antigenic shifts when a new virus is introduced into the human population through zoonotic transmission. The dynamics of the epidemic is closely related to the antigenic structure and evolution of the viral population. The spreading of multiple strains may be investigated by means of mathematical models, and four studies have recently uncovered the role of a ‘reinfection threshold’ (Gomes *et al* 2005) in regulating pathogen diversity (Gomes *et al* 2002; Boni *et al* 2004; Abu-Raddad & Ferguson 2004; Gökaydin *et al* 2005). In spite of the significant differences in model formulations, assumptions, and propositions, there is a striking convergence at the level of the underlying mechanisms and results: levels of infection increase abruptly as a certain threshold is crossed, increasing the potential for pathogen diversity. This may be achieved by increasing the transmissibility (modelled by  $R_0$  in this work), by decreasing the strength of the immunity (modelled by increasing  $\sigma$  in this work) or by increasing the rate at which novel pathogen variants are generated (not considered in this work).

The concept of reinfection threshold was introduced in the context of a mean field model for vaccination impact (Gomes *et al* 2004) and has been the subject of some debate (Breban and Blower 2005), on the grounds that it corresponds to a change in the order of magnitude of the equilibrium density of infectives that takes place over a certain range of parameter values, rather than at a well defined threshold. In contrast with other phenomena in epidemic models where the term threshold is widely used, the reinfection threshold does not correspond to a bifurcation, or a phase transition, occurring at a well defined critical value. In Section 2, we give a precise definition of the reinfection threshold concept, relating it to a bifurcation that takes place in the limit when the demographic renewal rate tends to zero. Thus, the reinfection threshold is a smoothed transition that occurs in systems with low birth and

death rates, where a pronounced change in the systems' steady state values takes place over a narrow range in parameter space, akin to a smoothed phase transition in finite physical systems around the value of the critical control parameter where a sharp transition occurs in an infinite system. This approach reconciles the two opposing views in the literature, and we shall use the term reinfection threshold throughout the paper in this sense.

For the invasion by a pathogen strain of a homogeneously mixed population where another strain circulates, it was recently found that strain replacement is favoured when the transmissibility is below the reinfection threshold, while coexistence is favoured above (Gökaydin *et al* 2005). Here we consider a model of contact structure in the host population to describe the underlying network for disease transmission, and investigate how this impacts on the outcome of an invasion by a new strain, that starts by infecting a very small fraction of the population.

Regular lattices are simple models that account for the geographical distribution of the host population through local correlations but are not good descriptions of social contact networks as they neglect mobility patterns. By contrast, random graphs are simple models of complex networks that account for the mobility of the host population, through the random links or connections, but by neglecting local correlations render these models poor descriptions of real social networks. A more realistic model of social networks was proposed recently by Watts and Strogatz. In 1998 they introduced small-world networks with topologies that interpolate between lattices and random graphs (Watts & Strogatz 1998). In these networks a fraction of the lattice links is randomized by connecting nodes, with probability  $p$ , with arbitrary nodes on the lattice; the number of links is preserved by removing lattice links when random ones are established. This interpolation is non linear: for a range of  $p$  the network exhibits small-world behaviour, where a local neighbourhood (as in lattices) coexists with a short average path length (as in random graphs). Analysis of real networks (Dorogotsev & Mendes 2002) reveals the existence of small-worlds in many interaction networks, including networks of social contacts. In a recent work the contact patterns for contagion in urban environments have been shown to share the essential characteristics of the Watts and Strogatz small-world model (Eubank *et al* 2004).

In this work, we implement the infection dynamics on a small-world network and find that the contact structure of the host population, parametrized by  $p$ , plays a crucial role in the final outcome of the invasion by a new strain, as departures from the homogeneously mixed

regime favour strain replacement and extinction versus coexistence (Section 3). Within the scope of an effective mean-field model (Section 4), this effect is attributed to a reduction of the effective transmissibility due to screening of infectives, resulting in a translocation of the reinfection threshold to higher transmissibility and thus decreasing the range where strain coexistence is the preferred behaviour.

This conclusion seems to contradict the established idea that localized interactions promote diversity, in the sense that the coexistence of several competing strains is favoured with respect to homogeneously mixed models. For the problem that we address here, this idea was confirmed in a recent work (Buckee *et al* 2004) where strain competition in small-world host networks has been considered. In Buckee *et al*, individual based stochastic simulations for a model with short term immunity, and thus high rates of supply of naive susceptibles, have shown that a localized host contact structure favours pathogen diversity, by reducing the spread of acquired immunity throughout the population. Our results indicate that when the rate of supply of susceptibles is low enough, the effect of localized interactions reported by Buckee *et al* is superseded by that of the reduction of the effective transmissibility, that places all but the most infectious strains below the reinfection threshold. Thus, in the case of long lasting partial immunity, a predominantly local contact structure will contribute to reduce the number of coexisting competing strains in the host population.

## II. ANALYSIS OF THE MEAN FIELD MODEL

We consider an antigenically diverse pathogen population with a two-level hierarchical structure: the population accommodates a number of strains (two in this work); each strain consists of a number of variants (here conceptualised as many). Variants in the same strain differ by some average within-strain antigenic distance,  $\sigma$ , and different strains are separated by some antigenic distance,  $\sigma_{\times}$ . Antigenic distance is negatively related to cross-immunity and, in some appropriate normalised measure, we may take  $0 \leq \sigma < \sigma_{\times} \leq 1$ . These assumptions are consistent with the idea that rapidly evolving RNA viruses experience selection as groups of antigenically close strains (Levin *et al* 2004). Studies of influenza A viral sequence evolution (Plotkin *et al* 2002; Smith *et al* 2004) provide empirical support of this modelling approach.

We consider a community of  $N$  (fixed) individuals, with susceptibles and infectives in

circulation. We assume that hosts are born fully susceptible and acquire a certain degree of immunity as they are subsequently infected. Individuals are characterized by their present infection status (healthy or infected by strain  $k$ ) and their history of past infections (previously infected by a set of strains). In this model the dynamics of a single viral strain, representing a group of cocirculating antigenically close strains, is described by a Susceptible-Infected-Recovered (SIR) model with partial immunity against reinfection. Abu-Raddad & Ferguson (2004) have proposed a different modelling approach based on the reduction of a multi-strain system to an ‘equivalent’ single strain SIR model, with parameters calculated to reproduce the values of the total disease prevalence and incidence of the original multi-strain model. In our model, the overall performance of a strain depends on a single parameter, the degree of immunity, measured by  $\sigma$ , for subsequent infections, and the role and meaning of the reinfection threshold (see below for a definition) become particularly clear.

The densities (or fractions of the host population) are denoted by  $s_j$  for susceptibles and  $i_j^k$  for infectives. The superscript  $k$  of  $i$  denotes the viral strain that currently infects that fraction of the population. The subscripts  $j$  describe the history of past infections (in the case of infectives, if different from the current infecting strain) and, for the model with two viral strains, run over the subsets of  $\{1, 2\}$ , that we will represent by  $j = 0, 1, 2, 12$ , for the susceptibles. For the infectives,  $j$  takes the values 0, 1 or 2.

The total fraction of the population infected by a given viral strain  $k$  is  $i^k = i_0^k + i_j^k$ ,  $k, j = 1, 2$ ,  $k \neq j$ , and infection of fully susceptible individuals occurs at a rate per capita (force of infection) given by  $\beta_k i^k$ . The parameter  $\beta_k$  is the transmissibility for strain  $k$ . Previous infections by the same strain reduce the transmissibility by a factor  $\sigma$  while previous infections by a different strain reduce the transmissibility by a factor  $\sigma_\times$ . Constant and equal birth/death rates,  $\mu$ , and constant recovery rate  $\gamma$ , are also assumed.

The mean-field equations for the dynamics of the various densities of susceptibles and infectives are

$$\begin{aligned} \frac{ds_0}{dt} &= \mu(1 - s_0) - (\beta_1 i^1 + \beta_2 i^2) s_0 \\ \frac{ds_j}{dt} &= -\mu s_j + \gamma i_0^j - (\sigma_\times \beta_k i^k + \sigma \beta_j i^j) s_j \quad j, k = 1, 2; j \neq k \\ \frac{di_0^k}{dt} &= -(\gamma + \mu) i_0^k + \beta_k i^k (s_0 + \sigma s_k) \quad k = 1, 2 \end{aligned}$$

$$\frac{di_j^k}{dt} = -(\gamma + \mu)i_j^k + \beta_k i^k (\sigma_\times s_j + \sigma s_{12}) \quad j, k = 1, 2; j \neq k \quad (1)$$

where the density of susceptibles that were previously infected with both viral strains is  $s_{12} = 1 - s_0 - s_1 - s_2 - i_1 - i_2$ . The parameter  $\mu$  is fixed at  $\mu = 1/80yr^{-1}$  corresponding to a life expectancy of 80 years and the rate of recovery from infection is also fixed at  $\gamma = 52yr^{-1}$  representing an average infectious period of approximately one week.

It is well known (Anderson & May 1991) that a given single strain,  $k$ , persists at endemic equilibrium if  $\beta_k > \gamma + \mu$  or, equivalently,  $R_k > 1$  where  $R_k$  is the basic reproduction number of strain  $k$ ,

$$R_k = \frac{\beta_k}{\gamma + \mu}. \quad (2)$$

The type of endemic equilibrium for the system described by (1) depends on the values of the transmissibilities,  $\beta_k$  (or  $R_k$ ). To establish whether two strains cocirculate at equilibrium, we evaluate the eigenvalues of the Jacobian at the single strain endemic equilibrium. If at least one of the eigenvalues is positive, the single strain equilibrium is unstable, and either coexistence or the other strain alone is the stable state. Applying this to strain 1, we find that this strain is expected to circulate alone when the pair  $(R_1, R_2)$  is in the region marked 1 in Figure 1(a,b). Likewise, strain 2 is expected to circulate alone in region 2. The regions shaded in grey are then identified as the set of parameter values for which coexistence of both strains is stable, or coexistence regions. For comparison, we include the dashed lines that delimit the wider coexistence regions in the absence of reinfection by the same strain ( $\sigma = 0$ ). The two panels correspond to systems with  $\sigma = 0.25$ , and different values of  $\sigma_\times$ :  $\sigma_\times = 0.27$  (or  $\delta\sigma := \sigma_\times - \sigma = 0.02$ ) in Figure 1(a); and  $\sigma_\times = 0.45$  (or  $\delta\sigma = 0.2$ ) in Figure 1(b). Comparing the two panels we make the expected observation that the stability of the coexisting solution is enhanced when the two strains are distantly related. We note the existence of two small ‘shoulders’ or ‘kinks’, marked A and B, on the boundaries of the coexistence regions. By numerical inspection, the kinks are found to be close to

$$\begin{aligned} A : \quad R_1 &= \frac{1}{\sigma}, R_2 = \frac{1}{\sigma_\times}, \\ B : \quad R_1 &= \frac{1}{\sigma_\times}, R_2 = \frac{1}{\sigma}. \end{aligned} \quad (3)$$

This makes intuitive sense. A simple SIR model with partial immunity (where reinfection occurs at a rate reduced by  $\sigma$ ) and with a low birth and death rate  $\mu$  (as considered here)

predicts a sharp increase in the density of infected individuals at  $R_0$  close to  $1/\sigma$  (Gomes *et al* 2004, 2005). This region of abrupt change is related to a bifurcation at  $R_0 = 1/\sigma$  that occurs when  $\mu = 0$ . We shall use the term reinfection threshold for the smoothed transition that takes place at small  $\mu$ , as well as for the approximate locus  $R_0 = 1/\sigma$  of this crossover. Focussing on strain 1, we expect a step increase in the infections by strain 1 as  $R_1$  increases beyond  $R_1 = 1/\sigma$ , enhancing the competitive advantage of strain 1 relative to strain 2 and reducing the coexistence region. Two limiting cases deserve special reference: when  $\sigma$  is as large as  $\sigma_\times$ ,  $A = B$  and the coexistence region collapses to the diagonal; and when  $\sigma \rightarrow 0$  as in previously studied models (May & Anderson 1983; Bremerman & Thiemme 1989) the coexistence region is maximal.

Hereafter we will restrict ourselves to a symmetrical model, and will denote  $R_1 = R_2$  by the usual symbol for the basic reproduction number,  $R_0$ . Figure 1(c,d) shows the stability of the coexistence equilibrium as a function of  $R_0$ , measured by the real parts of the seven eigenvalues of the linear approximation of system (1) at equilibrium for  $\sigma = 0.25$  and  $\delta\sigma = 0.02$  (Figure 1(c)),  $\delta\sigma = 0.2$  (Figure 1(d)). All the eigenvalues have negative real parts, and all but the smallest of them change by several orders of magnitude as  $R_0$  crosses the reinfection threshold region around  $R_0 = 1/\sigma$ . The plot shows the modulus of the real parts of the seven eigenvalues, in logarithmic scale, versus  $R_0$ , and the vertical line through  $R_0 = 1/\sigma$  marks the position of the reinfection threshold. Also shown by the dashed line is the total density of infectives at the equilibrium, which also increases by two orders of magnitude as  $R_0$  crosses the reinfection threshold region.

In both cases we observe that as the transmissibility crosses the reinfection threshold around  $R_0 = 1/\sigma$  the overall stability of the coexistence equilibrium increases significantly, as the largest eigenvalues decrease steeply. This effect is achieved by increasing either  $R_0$  or  $\sigma$ , and the system behaviour can be characterised in terms of  $R_0$  or of  $\sigma$ . Throughout the rest of this work we fix  $R_0$  and vary  $\sigma$ .

The behaviour of the solutions of (1) for  $\delta\sigma = \sigma_\times - \sigma = 0.02$  and  $\delta\sigma = 0.2$  is shown in Figures 2 and 3. We have taken  $\sigma = 0.2$ ,  $\sigma = 0.25$  and  $\sigma = 0.3$  in panels a), b) and c), respectively, corresponding to below threshold, threshold and above threshold behaviour for the fixed value of  $R_0 = 3.9$ . By threshold we mean, as before, the window of parameter values around  $R_0 = 1/\sigma$  that corresponds to the smoothed transition that takes place for small birth and death rate  $\mu$ , where the systems' coexistence equilibrium densities and stability

properties change very rapidly. This is illustrated in the panels d), e) and f) of Figures 2 and 3, where the dashed line is at  $R_0 = 3.9$  and the dotted line indicates the position of the reinfection threshold  $R_0 = 1/\sigma$ , for  $\sigma = 0.2$  (Figure 2(d) and 3(d)),  $\sigma = 0.25$  (Figure 2(e) and 3(e)) and  $\sigma = 0.3$  (Figure 2(f) and 3(f)). The full line depicts the total equilibrium density of infectives with either one of the two strains as a function of  $R_0$  for the (unique) stable steady state of the system, corresponding to endemic equilibrium where both viral strains coexist at the same steady state densities.

The numerical integration of equations (1) starts with a single circulating strain (strain 1), and when the single strain steady state is reached at  $t \sim 20$  years a small fraction ( $1.5 \times 10^{-4}$ ) of individuals infected with the invading strain (strain 2) is introduced in the system. The two curves in panels a), b) and c) of Figures 2 and 3 represent, in logarithmic scale, the infective densities for each of the strains as a function of time obtained from this numerical integration. The curve that corresponds to the density of infectives carrying strain 2 starts at  $t \sim 20$  years with density  $1.5 \times 10^{-4}$  in all the examples shown.

On relatively short time scales of a few decades, we find that the reinfection threshold is the boundary between two different regimes. For very similar viral strains, as depicted in Figure 2, the behaviour of the model below threshold is strain replacement, and the behaviour on and above threshold is strain coexistence. For distinct viral strains, as in Figure 3, the outcome is always strain coexistence, but the density oscillations are negligible above threshold, and very pronounced below threshold. In order to extract epidemiologically significant predictions from the mean field model we have to take into account that the population is discrete, and that densities below a certain lower bound, that depends on the population size, are effectively zero. If we take this effect into account and set the densities to zero when they fall below  $10^{-6}$ , we obtain extinction of both strains in the case of Figure 3(a).

For longer time scales, however, the model also predicts coexistence for the case of similar strains below threshold (Figure 2(a)) since there are no attractors in the single strain invariant subspaces when the two strains have the same transmissibility. All the solutions that were analysed tend eventually to the coexistence equilibrium, but the transients for similar strains below threshold last for several hundred years, during which the density of infectives carrying strain 1 reaches much smaller values than the cut-off of  $10^{-6}$ .

This behaviour and the role of the reinfection threshold can be interpreted in terms of

the eigenvalues of the coexistence endemic equilibrium represented in Figure 1(c,d). As  $R_0$  increases across the threshold, the real parts of the eigenvalues decrease steeply, and the imaginary parts vanish. As a result the oscillatory component of the system plays an important role below the reinfection threshold and is absent above. This is the basic ingredient of the different invasion dynamics depicted in Figures 2 and 3.

The difference in below threshold behaviour between similar and dissimilar strains, strain replacement in the former case and total extinction in the latter may be understood intuitively in terms of the reduced cross-immunity of dissimilar strains. In this case, the small fraction of infectives carrying strain 2 finds a highly susceptible population and generates a large epidemic outbreak, during which strain 1 goes extinct because of the lack of susceptibles. Strain 2 quickly exhausts its pool of susceptibles through first infections, and then dies out too as  $\sigma R_0 < 1$ .

Then, for realistic population sizes, the predictions of the mean-field model are the following. For similar viruses, strain replacement (drift) occurs below threshold, and coexistence on and above threshold. For dissimilar viruses, global extinction occurs below threshold while coexistence occurs on and above threshold.

It is known (Bayley 1975) that fluctuations due to stochastic effects in discrete populations will also favour strain extinction and replacement with respect to deterministic model predictions. A homogeneously mixed stochastic version of model (1) was considered by Gökaydin *et al* (2005) for population sizes between  $10^6$  and  $10^8$ , and, as expected, stochasticity was found to favour strain replacement and extinction both for similar and dissimilar strains. This effect may be, however, greatly enhanced in more realistic descriptions of the host population where the homogeneously mixed assumption is relaxed.

### III. DRIFT AND SHIFT IN SMALL-WORLD NETWORKS

In the presence of random long-range links such as those considered in small-world networks the endemic and epidemic thresholds of Susceptible-Infective-Susceptible (SIS) and SIR models may be mapped on to *mean-field* site and bond percolation transitions (Grassberger 1983, Dammer & Hinrichsen 2003, Hastings 2003). In recent works, the network topology has been considered in the calculation of endemic and epidemic thresholds of SIS and SIR models (May & Lloyd 2001, Moore & Newmann 2000a, 2000b, Pastor-Santorras

& Vespigniani 2001a) and the results revealed a strong dependence of the threshold values on the network size and structure. The contact network topology has also been shown to play an important role in the stationary properties of the endemic state (Pastor-Santorras & Vespigniani 2001b), the short term dynamics of epidemic bursts (Keeling 1999, Kleczkowski & Grenfell 1999, Rhodes & Anderson 1996), the long term dynamics of childhood diseases (Verdasca *et al* 2005) and in the estimation of disease parameters from epidemiological data (Meyers *et al* 2005).

The structure of the network of contacts of the host population is also expected to play a role in the invasion dynamics described in the previous section. This will affect the pattern of strain replacement and as a consequence the evolution of competing multi-strain pathogens. In the following we analyse quantitatively the effects of a network of social contacts with small-world topology on the simple two strain model (1).

We implemented a discrete version of the model (1) on a cellular automaton (square lattice) with  $N = 800 \times 800$  sites and small-world interaction rules (see the appendix for a description of the algorithm). We started by simulating the behaviour of the system for a single strain model, whose mean field equations are simply

$$\begin{aligned}\frac{ds_0}{dt} &= \mu(1 - s_0) - \beta i s_0 \\ \frac{di}{dt} &= -(\gamma + \mu)i + \beta i(s_0 + \sigma(1 - s_0 - i))\end{aligned}\tag{4}$$

We found characteristic medium and long-term dynamics related, in a quantitative fashion, to the structure of the network of contacts. In particular, as  $p$  decreases, the increase in spatial correlations (i) decreases the effective transmissibility through the screening of infectives and susceptibles, which in turn increases the value of the transmissibility at the endemic and reinfection thresholds. In addition, the spatial correlations (ii) enhance the stochastic fluctuations with respect to the homogeneously mixed stochastic model. This effect is particularly strong at low  $p$ , where the relative fluctuations are largest and where as a consequence (iii) the dependence of the steady state densities on the effective transmissibility predicted by the mean-field equations breaks down. Analogous effects, including departures from the mean-field behaviour at the endemic threshold (persistence transition) of a SIR model with non-zero birth rate have been reported recently (Verdasca *et al* 2005).

In Figure 4 we plot the effective transmissibility,  $\beta_{eff}$  (average density of new infectives per time step divided by the value of  $i(s_0 + \sigma(1 - s_0 - i))$  for the instantaneous densities), at

fixed  $R_0 = 3.9$  and  $\sigma = 0.30$ , well above the reinfection threshold of the mean-field model, as a function of the small-world parameter,  $p$ . The variation of the effective transmissibility with  $p$  is due to the clustering of infectives and susceptibles. This is a well known screening effect that results from the local structure (correlations), and has to be taken into account in fittings to effective mean-field models. In this framework, the reduction of the effective transmissibility represents an increase of the value of  $R_0$  at the reinfection threshold.

The clustering, and spatial correlations in general, have also drastic consequences on the amplitude and nature of the stochastic fluctuations. Enhanced fluctuations will ultimately lead to stochastic extinction as  $p$  decreases, but before extinction occurs, the fluctuations lead to the appearance of a regime dominated by local structure and correlations, where the mean-field relations among the equilibrium densities break down. This is illustrated in Figure 5 where we plot the effective transmission rate (dots) as a function of the equilibrium density of infectives (model parameters as in Figure 4). In the same figure we plot the equilibrium value of the density of infectives (full line) predicted by the mean-field equations (4) for a value of the transmissibility equal to the effective transmissibility obtained from the simulations. When  $p > p_b$ , away from the network endemic threshold at  $p = p_c$ , the mean-field equilibrium density for the effective transmissibility is in excellent agreement with the simulated equilibrium density. In the region of small  $p$  ( $p_c < p < p_b$ ), however, the simulated equilibrium densities differ significantly from those calculated using the effective mean-field theory. A departure from the mean-field dependence of the effective transmissibility on the steady state density of infectives implies that the description of the system is no longer possible in terms of effective mean-field theories based on density dynamics, by contrast with the second regime where the contact structure can be implicitly taken into account by effective mean-field models (Section 4).

We then focussed on the analysis of the invasion dynamics. We performed individual based simulations starting from an initial condition where the system is close to the steady state for a single resident strain and introduced a small fraction of individuals ( $1.5 \times 10^{-4}$ ) infected by the invading strain. The algorithm is a natural extension of the single strain stochastic algorithm for SIR dynamics with reinfection on a small-world network of contacts, and a detailed description is given in the appendix. We found that as local effects become important (low  $p$ ), strain replacement (and also total extinction) are favoured with respect to the homogeneously mixed regime ( $p = 1$ ). These results are summarized in Figure 6

where we plot  $\sigma$  at crossover between the different regimes, coexistence, replacement and extinction, versus the small-world parameter,  $p$ , for systems where the competing viral strains are similar,  $\delta\sigma = 0.02$  (Figure 6(a)) and dissimilar,  $\delta\sigma = 0.2$  (Figure 6(b)). The full line is the boundary between the strain coexistence and the strain replacement regimes, and the dashed line is the boundary between strain replacement and total extinction. The final outcome of an invasion is determined by carrying out a series of simulations, for different values of  $p$  and  $\sigma$ , and keeping  $R_0$  fixed at 3.9. For each  $(p, \sigma)$ , twenty (forty in some cases) invasion simulations are performed for a period of 13.7 years, with invasion at  $t = 4.1$  years. The fraction of simulations where both the circulating and the invading strain prevail is plotted as a function of  $\sigma$ , at fixed  $p$ . This fraction changes rapidly from one to zero as  $\sigma$  decreases across a small interval, and the boundary of the coexistence regime (the full line in Figure 6(a,b)) is determined as the point where it takes the value 0.5. A similar analysis yields the boundary that separates the replacement from the total extinction regime (the dashed line in Figure 6(a,b)). The results show that as  $p$  decreases the value of  $\sigma$  at these two boundaries increases exponentially from its value in the homogeneously mixed system,  $p = 1$ . As a consequence, the range of parameters in the coexistence regime decreases drastically as  $p$  decreases, supporting the claim that the structure of the small-world network of contacts hinders, rather than favours, pathogen diversity.

This contrasts with the behaviour reported by Buckee *et al* (2004) for a model of strain evolution including short term host immunity and cross-immunity on a (static) small-world network of contacts, where coexistence of competing strains was found to be favoured with respect to the homogeneously mixed model. The different behaviour we report is due to the combined effect of small-world network structure and a low rate of supply of naive susceptibles, and may be understood in terms of the analysis of the single strain stochastic model discussed previously, together with the behaviour of the two-strain mean-field model which, for low  $\mu$ , predicts strain coexistence as the outcome of an invasion only when the transmissibility is high enough.

Recall that in the mean-field model of Section 2 (system (1)) when a second strain is introduced in a population with a resident virus, drift occurs below the reinfection threshold for antigenically similar strains (small  $\delta\sigma$ ). When the resident and the invading strains are antigenically distant (large  $\delta\sigma$ ) the final outcome is coexistence at and above the reinfection threshold and global extinction below threshold. The results of the individual based

simulations show that the enhancement of the stochastic fluctuations due to spatial correlations favours replacement where we would otherwise have coexistence, and global extinction where we would otherwise have replacement. In particular, replacement (both drift and shift, replacement of dissimilar strains) becomes a typical outcome at the reinfection threshold, instead of coexistence as in the mean-field model. This may be viewed as a finite size stochastic effect similar to the effect reported in Gökaydin *et al* 2005 for the homogeneously mixed stochastic model, or to what we have also found here for  $p = 1$ , but much more pronounced. As we noted previously the amplitude of the stochastic fluctuations at small values of  $p$  is greatly enhanced with respect to the amplitude of the stochastic fluctuations at  $p = 1$ , due to coherent fluctuations of host population clusters.

However, the main effect of spatial correlations that accounts for the results of Figure 6 is the screening of infectives that leads to the reduction of the effective transmissibility as shown in Figure 4. As  $p$  decreases, this effect brings a system above the reinfection threshold closer to or even below the reinfection threshold, also favouring replacement for small  $\delta\sigma$  and either replacement or extinction for larger  $\delta\sigma$ . While the effects of the coherent fluctuations of clusters are important only in a small range of  $p$  above the single strain endemic transition, screening of infectives occurs over the whole range of  $p$  with the corresponding translocation of the reinfection threshold to larger values of  $R_0$ . In particular, for a large range of values of  $p$  we obtain drift/shift, instead of coexistence as predicted by the well mixed model for the same disease parameters. Many of these effects may be captured by effective mean-field models as described in the next section.

#### IV. AN EFFECTIVE MEAN-FIELD MODEL

In Section 3 we have seen that, for single strain dynamics, the mean field equilibrium incidence given by (4) for the effective transmissibility is in excellent agreement with the results of the simulations for values of the small world parameter  $p$  in an interval  $[p_b, 1]$ , while departure from the mean field relations occurs close to the endemic transition threshold at  $p_c < p < p_b$  (see Figure 5).

In this section we show that, for the full system and  $p$  in the range  $[p_b, 1]$ , the simulated time series are well approximated by the solutions of an effective mean-field model of the form (1). For the construction of the effective model we assume that the transmissibility

is of the form  $\beta_{eff} = \beta f(p)$ , where  $f(p)$  is a function, unknown a priori, that represents the screening of infectives. The screening function  $f(p)$  is obtained from a plot  $\beta_{eff}(p)$  as in Figure 4, where the screening effect is quantified for the single strain dynamics. The relevant range of  $p$  for this fit is  $[p_b, 1]$ , since the breakdown of the mean field equilibrium relations implies that our ansatz for the form of the infection rate is no longer valid. Even in this range it is not obvious that the ansatz will yield an effective mean-field model capable of describing the full dynamical behaviour of the simulations when a resident and an invading strain interact.

In Figure 7(a), black line, we show the results of stochastic invasion simulations as described in Section 3 and in the Appendix, for  $p = 0.5$  (other parameters as in Figure 2.b)), together with the numerical integrations, grey line, of the coupled strain effective mean-field model, given by (1) with  $\beta_k = \beta_{eff}$ , for  $k = 1, 2$ . Also shown in Figure 7(b) are, for comparison, the solutions of the standard mean-field model, where  $f(p) = 1$  (grey line), plotted together with the stochastic simulations of Figure 7(a) (black line). In all cases we use the same initial conditions and the same invasion conditions.

While the standard mean-field model disagrees quantitatively, and even qualitatively, with the results of the simulations, the effective mean-field model describes accurately the dynamical behaviour of the system, except for the stochastic fluctuations about the average densities.

Systematic calculations show that the effective mean-field model performs rather well against simulations, everywhere in the region where the mean-field relations apply. In this regime, the effect of the contact structure of the host population is accurately described through the screening function  $f(p)$ , obtained from the steady state averages of single strain simulations.

In the range  $[p_c, p_b]$  of  $p$  above the endemic threshold where we have found significant departures from the mean-field description, one may think that a more general ansatz for the form of the force of infection could lead to a modified effective mean-field model, albeit a more complicated one, that would fit the simulation results. However, it is easy to check that the parametric plot of  $\beta_{eff}(p)$  vs  $i^*(p)$ , where  $i^*(p)$  is the steady state average infective density, follows the mean field relation of the model with linear force of infection whatever the functional form assumed for  $\beta(i, p)$ . Indeed, for any function  $\beta(i, p)$ , and rate of infection

of the form

$$\beta(i, p)i(s + \sigma(1 - s - i)), \quad (5)$$

$\beta_{eff}(p)$  measured from the simulations is  $\beta_{eff}(p) = \beta(i^*, p)$ , and the curve  $(\beta_{eff}(p), i^*(p))$  is the same as the standard mean field curve for  $\beta(i^*)$ . This means that even in the scope of a more general model with a nonlinear force of infection the mean field curve for  $\beta_{eff}(p)$  vs  $i^*(p)$ , the full line in Figure 5, does not fit the simulations results for  $p$  in the range  $[p_c, p_b]$ .

We conclude that the effect of the breakdown of the mean-field relations reported in Section 3 is an indication of a new regime where spatial correlations are too important for the contact rate between individuals of different classes to be described by the product of the corresponding densities. The construction of effective models in this regime requires the use of pair approximations that take into account the spatial correlations (de Aguiar *et al* 2003) and will be the subject of future work.

## V. CONCLUSIONS

We performed stochastic simulations of individual based models on small-world networks to represent host populations where one or two viral strains, each representing a group of antigenically close variants, may be present. In the case of a single viral strain, the node dynamics corresponds to a SIR model with reinfection at a reduced rate due to acquired immunity. In the case of two competing strains, the rate of infection by a distinct strain is also reduced due to cross immunity, which is always weaker than strain specific immunity. Both the single and the double strain models include crucial ingredients required by realistic modeling of the host population, namely stochasticity, a discrete finite population, and spatial structure given by a plausible contact network.

We analysed both the reinfection dynamics of the single strain model and the invasion dynamics of the two strains model, taking initial conditions that correspond to the presence of a small number of individuals infected with a pathogen strain in a population where another pathogen strain circulates.

For single-strain dynamics, we found that the major effect of spatial correlations is a decrease in the effective transmissibility through the screening of infectives and susceptibles which in turn increases the value of the transmissibility at the endemic and at the reinfection thresholds. In addition, spatial correlations enhance the amplitude of the stochastic fluctua-

tions with respect to the homogeneously mixed stochastic model. This effect is particularly strong at low  $p$ , where the relative fluctuations are largest and where the mean-field dependence of the steady state densities on the effective transmissibility breaks down. Indeed, we have found a regime at small  $p$ , where spatial correlations dominate and the mean-field relations break down, as well as a second, wider, regime for larger values of  $p$  where effective mean-field models are capable of describing the essential effects of the spatial correlations through a reduced effective transmissibility.

For the two-strain model, we found that the host contact structure significantly affects the outcome of an attempted invasion by another strain of a population with an endemic resident strain, and by contrast with standard expectations we observed that spatial structuring reduces the potential for pathogen diversity. The simulation results show that the structure of the network of contacts favours strain replacement (drift/shift) or global extinction versus coexistence as the outcome of an invasion, with respect to the mean-field and stochastic homogeneously mixed populations. In particular, we find that as the small-world parameter,  $p$ , decreases at fixed  $R_0$ , the value of the strain specific immunity parameter  $\sigma$  above which coexistence is the typical outcome increases exponentially from its value for the homogeneously mixed system,  $p = 1$ , supporting the claim that local correlations strongly reduce pathogen diversity.

This conclusion is in apparent contradiction with the established idea that localized interactions promote diversity, as confirmed by stochastic simulations for a model with high rates of supply of naive susceptibles. In that model the effect of the host contact structure favours pathogen diversity, by suppressing the uniform spread of acquired immunity throughout the population. By contrast, in our model characterised by partial permanent immunity and low rates of supply of naive susceptibles (through births) the former effect is superseded by the screening effect. The latter is also due to the clustering of the host population, and results in a reduction of the effective transmissibility, changing the reinfection threshold to higher levels of  $R_0$ , and therefore reducing the range where coexistence is the preferred behaviour.

The results of our simulations strongly support the conclusion that in systems with a reinfection threshold, due to a low rate of supply of naive susceptibles, the major effect of the host population spatial structuring is the effective reduction of pathogen diversity.

The immunity profile (Ferguson & al. 2003) and the duration of infection (Gog & Grenfell 2002) have recently been shown to play an important role in shaping the patterns of pathogen

evolution in multi-strain models with mutation generated antigenic diversity. Investigating the additional effect of host population contact structure topology in these models will be the subject of future work.

### Acknowledgements

Financial support from the Portuguese Foundation for Science and Technology (FCT) under contracts POCTI/ESP/44511/2002, POCTI/ISFL/2/618 and POCTI/MAT/47510/2002, and from the European Commission under grant MEXT-CT-2004-14338, is gratefully acknowledged. The authors also acknowledge the contributions of J. P Torres and M. Simões to test and to improve the code used in the simulations.

---

Abu-Raddad, L J and Ferguson, N F (2004) The impact of cross-immunity, mutation and stochastic extinction on pathogen diversity, *Proc. R. Soc. Lond. B* **271** 2431-2438.

de Aguiar, M A M, Rauch, E M, Bar-Yam, Y (2003) Mean field approximation to a host-pathogen model, *Phys. Rev. E* **67** 047102.

Anderson, R A and May, R M (1991) *Infectious Diseases of Humans*, Oxford U. P., Oxford.

Bailey, N T J (1975) *The Mathematical Theory of Infectious Diseases*, 2nd edition, Charles Griffin & Co, London.

Boni, M F, Gog, J R, Andreasen, V and Christiansen, F B (2004) Influenza drift and epidemic size: the race between generating and escaping immunity, *Theor. Popul. Biol.* **65** 179-191.

Bremermann, H and Thieme, H R (1989) A competitive-exclusion principle for pathogen virulence, *J. Math. Biol.* **27** 179-190.

Buckee, C O' F, Koelle, K, Mustard M J, and Gupta, S (2004) The effects of host contact network structure on pathogen diversity and strain structure, *Proceedings of the National Academy of Science* **101** 10839-10844.

Cane, P C (2001) Molecular epidemiology of respiratory syncytial virus, *Rev. Med. Virol.* **11** 103-116.

Dammer, S M and Hinrichsen, H (2003) Epidemic spreading with immunization and mutations, *Phys. Rev. E* **68** 016114.

- Dorogotsev, S N and Mendes, J F (2003) *Evolution of Networks*, Oxford: Oxford University Press.
- Grassberger, P (1983) On the critical behaviour of the general epidemic process and dynamical percolation *Math. Biosci.* **63** 157-172.
- Eubank, S, Guclu H, Anil Kumar V S, Marathe M V, Srinivasan A, Torockzcal Z and Wang N (2004) Modelling disease outbreaks in realistic urban social networks, *Nature* **429** 180-184.
- Ferguson, N M, Galvani, A P and Bush, R B (2003) Ecological and immunological determinants of Influenza evolution, *Nature* **422** 428-433.
- Gog, J R and Grenfell, B T (2002) Dynamics and selection of many-strain pathogens, *Proc. Natl Acad. Sci. USA* **99** 17209-17214.
- Gökaydin, D, Oliveira-Martins, J B, Gordo, I and Gomes, M G M (2005) The reinfection threshold regulates pathogen diversity: The unusual patterns of influenza A evolution (submitted).
- Gomes, M G M, Medley, G F and Nokes, D J (2002) On the determinants of population structure in antigenically diverse pathogens *Proc. R. Soc. Lond. B* **269** 227-233.
- Gomes, M G M, White, L J and Medley, G F (2004) Infection, reinfection, and vaccination under suboptimal immune protection: Epidemiological perspectives. *J. Theor. Biol.* **228** 539-549.
- Gomes, M G M, White, L J and Medley, G F (2005) The reinfection threshold, *J. Theor. Biol.* (in press).
- Hastings, M B (2003) Mean-Field and anomalous behaviour on a small world network, *Phys. Rev. Lett.* **91** 098701.
- Hay, A J, Gregory, V, Douglas, A R and Lin, Y P (2001) The evolution of human influenza viruses, *Philos. Trans. R. Soc. Lond. B* **356** 1861-1870.
- Iturriza-Gómara, M, Kang, G and Gray, J (2004) Rotavirus genotyping: keeping up with an evolving population of human rotaviruses, *J. Clin. Virol.* **31** 259-265.
- Keeling, M J (1999) The effects of local spatial structure on epidemiological invasions *Proc. R. Soc. Lond. B* **266** 859-867.
- Kleczkowski, A and Grenfell, B T (1999) Mean field type of equations for spread of epidemics: the small world model, *Physica A* **274** 355-360.
- Levin, S A, Dushoff, J and Plotkin, J B (2004) Evolution and persistence of influenza A and other diseases, *Math. Biosci.* **188** 17-28.
- May, R M and Anderson, R M (1983) Epidemiology and genetics in the coevolution of parasites

and hosts, *Proc. R. Soc. Lond. B* **219** 281-313.

May, R M and Lloyd, A L (2001) Infection dynamics on scale free networks, *Phys. Rev. E* **64** 066112.

Meyers, L A, Pourbohloul, B P, Newman M E J, Skowronski D M, Brunham R C (2005) Network theory and SARS: predicting outbreak diversity, *J. Theor. Bio.* **232** 71-81.

Moore, C and Newmann, M E J (2000) Epidemics and percolation in small world networks, *Phys. Rev. E* **61** 5678-5682.

Moore, C and Newmann, M E J (2000) Exact solution of site and bond percolation on small world networks, *Phys. Rev. E* **62** 7059-7064.

Pastor-Santorras, R and Vespigniani, A (2001) Epidemic spreading in scale free networks, *Phys. Rev. Lett.* **86** 3200-3203.

Pastor-Santorras, R and Vespigniani, A (2001) Epidemic dynamics and endemic states in complex networks, *Phys. Rev. E* **63** 066117.

Plotkin, J B, Dushoff, J and Levin, S A (2002) Hemagglutinin sequence clusters and the antigenic evolution of influenza A virus, *Proceedings of the National Academy of Science* **99** 6263-6268.

Rhodes, C J and Anderson, R M (1996) Persistence and dynamics in lattice models of epidemic spread, *J. Theor. Biol.* **180** 125-133.

Smith, D J, Lapedes, A S, de Jong, J C, Bestebroer, T M, Rimmelzwaan, G F, Osterhaus, A D and Fouchier, R A (2004) Mapping the Antigenic and Genetic Evolution of Influenza Virus, *Science* **305** 371-376.

Verdasca J, Telo da Gama, M M, Nunes, A, Bernardino, N R, Pacheco, J M and Gomes, M C (2005) Recurrent epidemics in small world networks, *J. Theor. Biol.* **233** 553-561.

Watts, D J and Strogatz, S H (1998) It's a small world, *Nature* **392** 440-442.

## VI. APPENDIX

### A. description of the algorithm

A community of  $N$  (fixed) individuals comprises, at time  $t$ , susceptibles and infectives in circulation. Hosts are born fully susceptible and acquire a certain degree of immunity as they are subsequently infected. We consider susceptibles and infectives that were previously infected by strain  $i$ ,  $S_i$  and  $I_i^k$ . The indices denote previous and current infections as in the text.

We consider a cellular automaton (CA) on a square lattice of size  $N = L^2$  with periodic boundary conditions. The (random) variables at each site may take one of eight values:  $S_0$ ,  $S_1$ ,  $S_2$ ,  $I_0^1$ ,  $I_0^2$ ,  $I_1^1$ ,  $I_2^1$  or  $S_{12}$ . The lattice is full. We account for local interactions/connections with  $k$  neighbouring sites, with  $k = 12$ , and long-range interactions/connections, with a small-world probability,  $p$ .

The transmissibility  $\beta$  is the sum of the local and long-range rates of transmission. First infection, within-strain and between-strains reinfection, recovery, birth and death occur stochastically, with fixed rates  $(\beta, \beta\sigma, \beta\sigma_\times, \gamma, \mu, \mu)$ . The recovery time  $(1/\gamma)$  sets the time scale. At each Monte Carlo (time) step,  $N$  random site updates are performed following a standard algorithm. The type of event, long or short-range infection, within and between-strains reinfections by strains 1 and 2, recovery, birth and death, is chosen with the appropriate frequency  $(\beta p, \beta(1-p), \beta p\sigma, \beta(1-p)\sigma, \beta p\sigma_\times, \beta(1-p)\sigma_\times, \gamma, \mu, \mu)$  and then proceeds as follows.

a. Long(short)-range first infection by 1 (2). A site is chosen at random; if the site is occupied by an  $I$  or an  $S$  other than  $S_0$  no action is taken. If the site is occupied by an  $S_0$ , one of the other lattice sites (or of its  $k$  neighbours for short-range infection) is chosen at random;  $S_0$  is infected by 1 (2) iff that site is an  $I^1$  ( $I^2$ ).

b. Long(short)-range between strain reinfection by 1 (2). A site is chosen at random; if the site is occupied by an  $I$  or an  $S$  other than  $S_2$  ( $S_1$ ) no action is taken. If the site is occupied by an  $S_2$  ( $S_1$ ), one of the other lattice sites (or of its  $k$  neighbours for short-range infection) is chosen at random;  $S_2$  ( $S_1$ ) is reinfected by 1 (2) iff that site is an  $I^1$  ( $I^2$ ).

c. Long(short)-range within strain reinfection by 1 (2). A site is chosen at random; if the site is occupied by an  $I$  or an  $S$  other than  $S_1$  ( $S_2$ ) or  $S_{12}$  no action is taken. If the

site is occupied by an  $S_1$  ( $S_2$ ) or  $S_{12}$  one of the other lattice sites (or its  $k$  neighbours for short-range infection) is chosen at random;  $S_1$  ( $S_2$ ) or  $S_{12}$  is reinfected by 1 (2) iff that site is an  $I^1$  ( $I^2$ ).

d. Recovery: a site is chosen at random; if the site is occupied by an  $I$  recovery occurs.

e. Death and birth: a site is chosen at random and death occurs regardless; the site is then (re-)occupied by an  $S_0$ . Death is linear in the densities and birth is independent of the densities.

We used systems with  $800 \times 800$  nodes.

## FIGURES

**FIGURE 1** Stability analysis. (a,b) Conditions for strain coexistence or competitive exclusion as described by the two strain mean-field model. The panels correspond to models with  $\sigma = 0.25$  and different values of  $\sigma_x$ : (a)  $\sigma_x = 0.27$ ; (b)  $\sigma_x = 0.45$ . The regions shaded in grey are the set of parameter values for which coexistence of both strains is stable, or coexistence regions. The dashed lines delimit the wider coexistence regions in the absence of reinfection by the same strain ( $\sigma = 0$ ). In region 1 (resp. 2), the single strain endemic equilibrium for strain 1 (resp. 2) is stable. (c,d) Modulus of the real parts of the seven eigenvalues of the coexistence equilibrium along the diagonal of (a,b) respectively, in logarithmic scale. Also shown is the total density of infectives at equilibrium (dashed line), and the position of the reinfection threshold (dotted line).

**FIGURE 2** Mean-field new infectives densities for the two strain model of equations (1-4) with  $\delta\sigma = \sigma_x - \sigma = 0.02$ . We have taken  $\sigma = 0.2$ ,  $\sigma = 0.25$  and  $\sigma = 0.3$  in panels a), b) and c), respectively, corresponding to below threshold, threshold and above threshold behaviour for the value of  $R_0 = 3.9$ . This is illustrated in the diagrams d), e) and f) where the dashed line is at  $R_0 = 3.9$  and the dotted line indicates the position of the reinfection threshold  $R_0 = 1/\sigma$ . The full line depicts the equilibrium total density of infectives,  $i^*$ , as a function of  $R_0$  for the stable steady state of the system, the endemic equilibrium where both viral strains coexist.

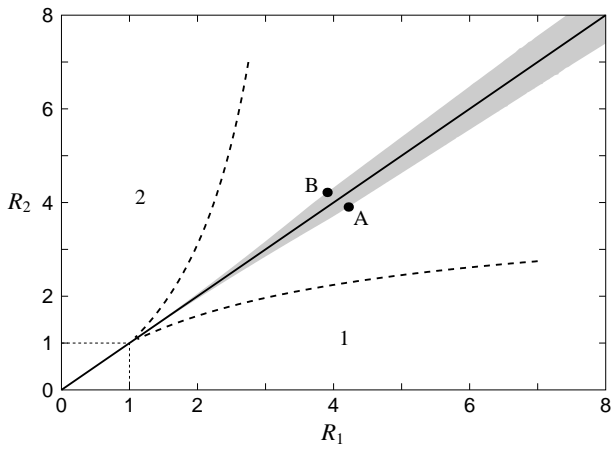
**FIGURE 3** Mean-field new infectives densities for  $\delta\sigma = 0.2$ . As in Figure 2 we take  $\sigma = 0.2$ ,  $\sigma = 0.25$  and  $\sigma = 0.3$  in panels a), b) and c), respectively, corresponding to below threshold, threshold and above threshold behaviour for  $R_0 = 3.9$ , as illustrated in the diagrams of panels d), e) and f).

**FIGURE 4** Effective transmissibility vs the small-world parameter,  $p$ . The effective transmissibility,  $\beta_{eff}$ , is calculated as the average density of new infectives per time step divided by  $i(s_0 + \sigma(1 - s_0 - i))$  where  $s_0$  and  $i$  are the instantaneous densities of susceptibles and infectives. The drastic reduction in  $\beta_{eff}$  is due to the clustering of infectives and susceptibles as  $p$  decreases and the spatial correlations increase. The model is the single strain reinfection model (4) and the parameters are  $R_0 = 3.9$  and  $\sigma = 0.3$ . The number of nodes is  $800 \times 800$ .

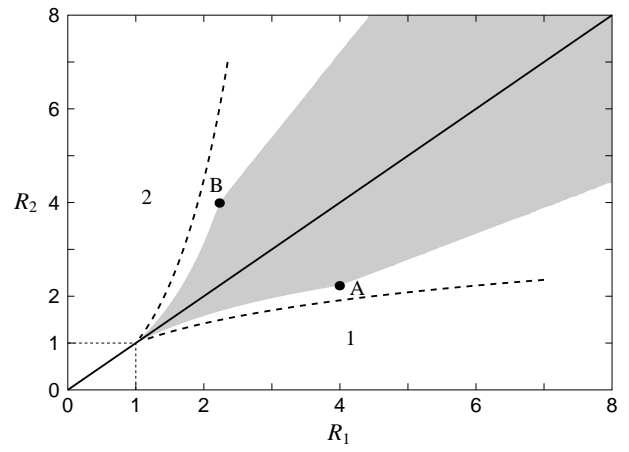
**FIGURE 5** Effective transmissibility vs the equilibrium infective density,  $i^*(p)$  (dots), over the whole range of the small-world parameter,  $p$  (dots). Notice the logarithmic scale in the  $i^*(p)$  axis. The full line is the  $\beta(i^*)$  curve calculated from the mean-field single strain reinfection model (4). The parameters are as in Figure 4. The results show the existence of two regimes: an effective mean-field regime for  $p > p_b$ , where the relations between the equilibrium densities are given by the mean-field equations for the screened value of the transmissibility, and a fluctuation dominated regime for  $p_c < p < p_b$ , where the mean-field relations break down.

**FIGURE 6** Coexistence versus replacement (full line) and replacement versus total extinction (dashed line) crossovers in  $(p, \sigma)$  space. The reinfection parameter,  $\sigma$ , is plotted as a function of the small-world parameter,  $p$ , at the crossover separating the dynamical regimes of coexistence of two competing viral strains (above the full line), of invasion prevalence (between the dashed and the full lines) and of total extinction (below the dashed line). See the text for details. Panel a) corresponds to similar strains,  $\delta\sigma = 0.02$ , and plot b) to dissimilar strains,  $\delta\sigma = 0.2$ .  $R_0 = 3.9$  and  $N$  as in other simulations.

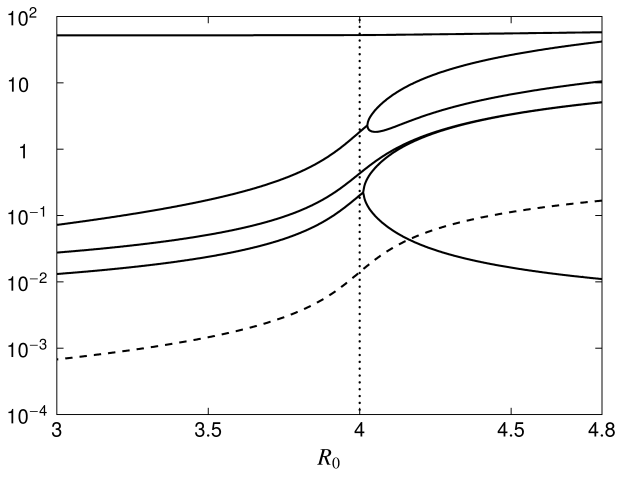
**FIGURE 7** Mean field and individual based description of invasion dynamics. The same initial conditions and the same invasion conditions are used in all cases. (a) Mean-field new infectives densities (grey line) for the model of equations (1) with  $\beta_k = \beta_{eff}$ ,  $k = 1, 2$ , fitted from the simulations of the single strain model for  $p = 0.5$  (other parameters as in Figure 2(b)), and time series (black line) of the stochastic model for  $p = 0.5$  (other parameters as in Figure 2(b)). (b) We also show, for comparison, the solutions of the standard mean-field model (grey line), where  $\beta_k = \beta$ ,  $k = 1, 2$ , are not corrected to take into account the screening. The black line corresponds to the same data as in (a).



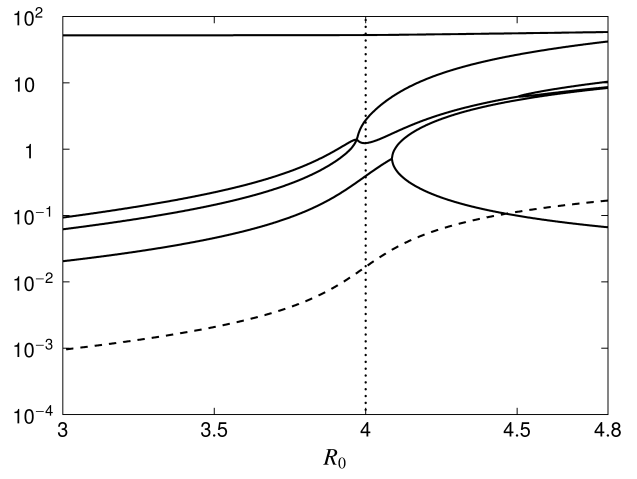
a)



b)

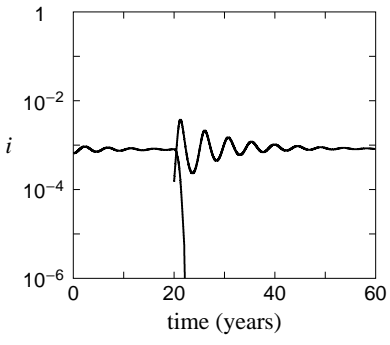


c)

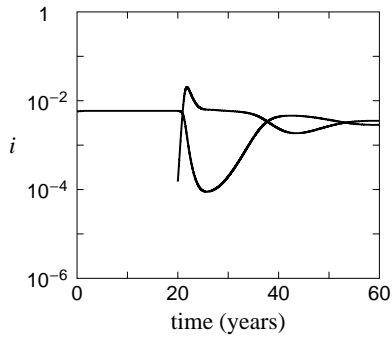


d)

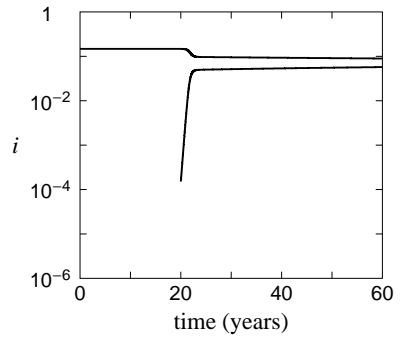
FIG. 1:



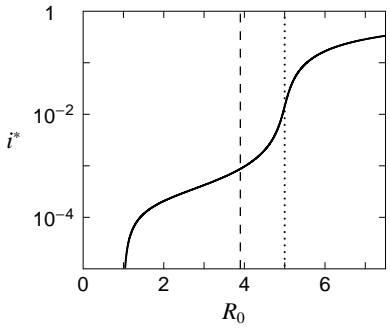
a)



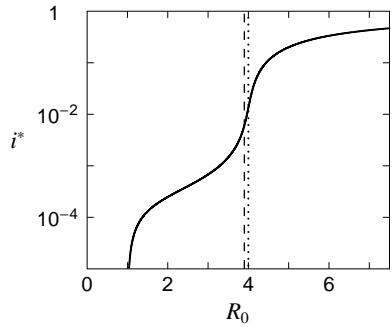
b)



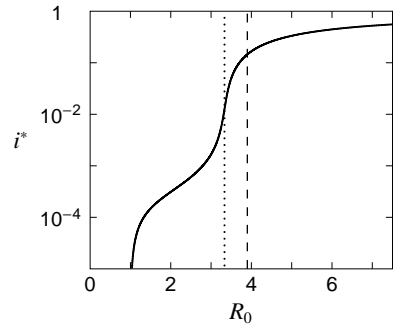
c)



d)



e)



f)

FIG. 2:

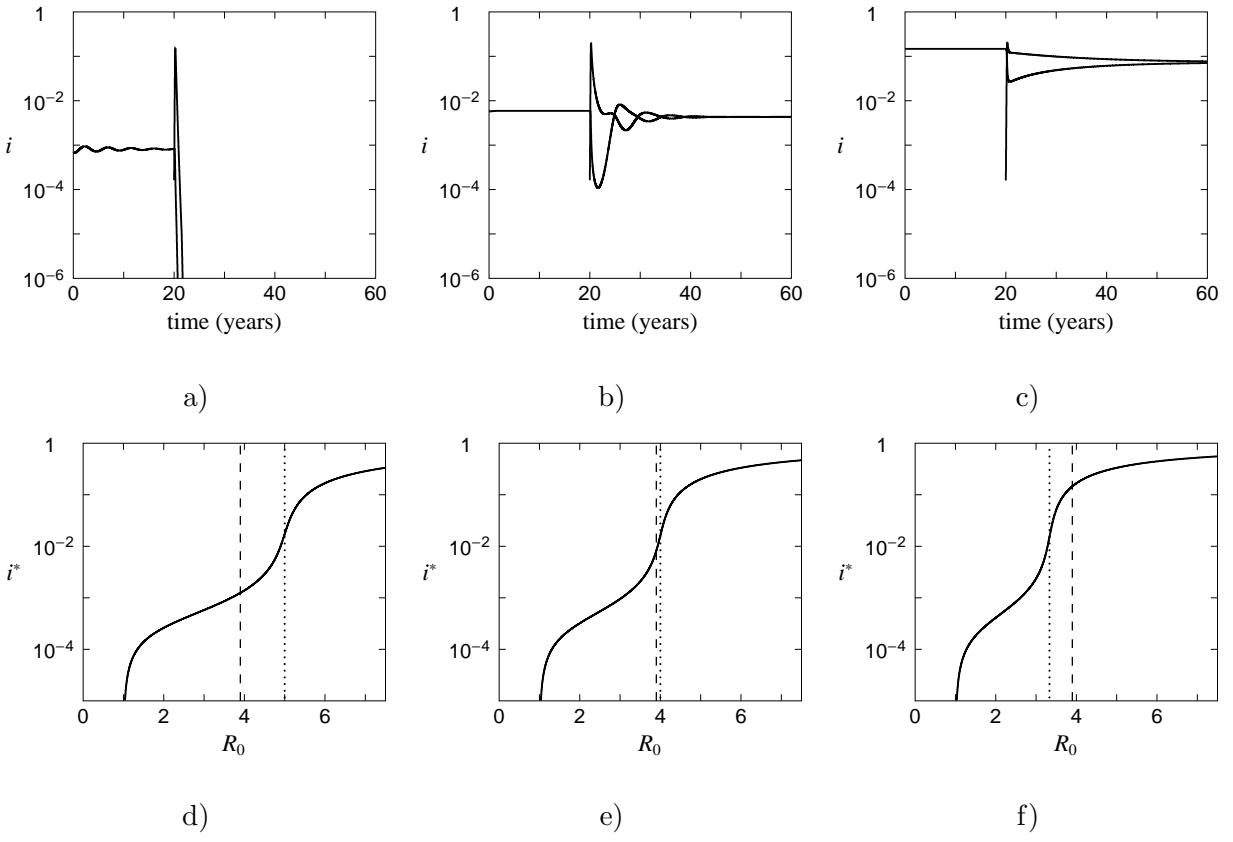


FIG. 3:

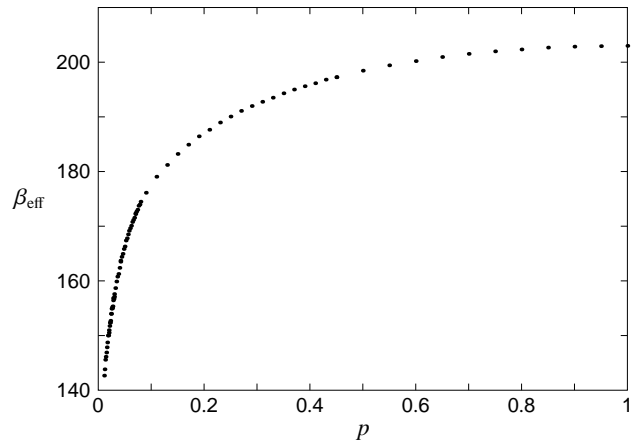


FIG. 4:

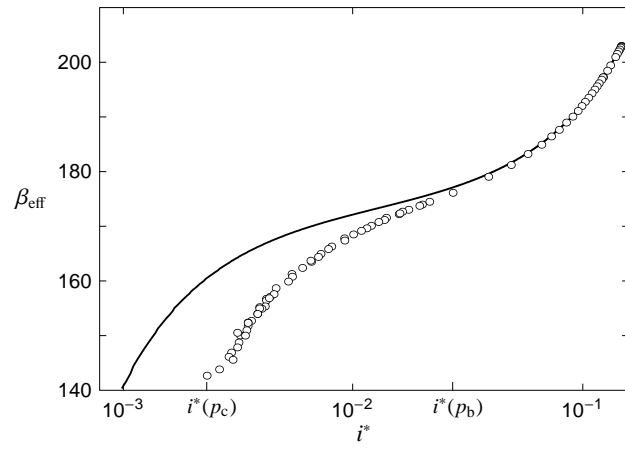


FIG. 5:

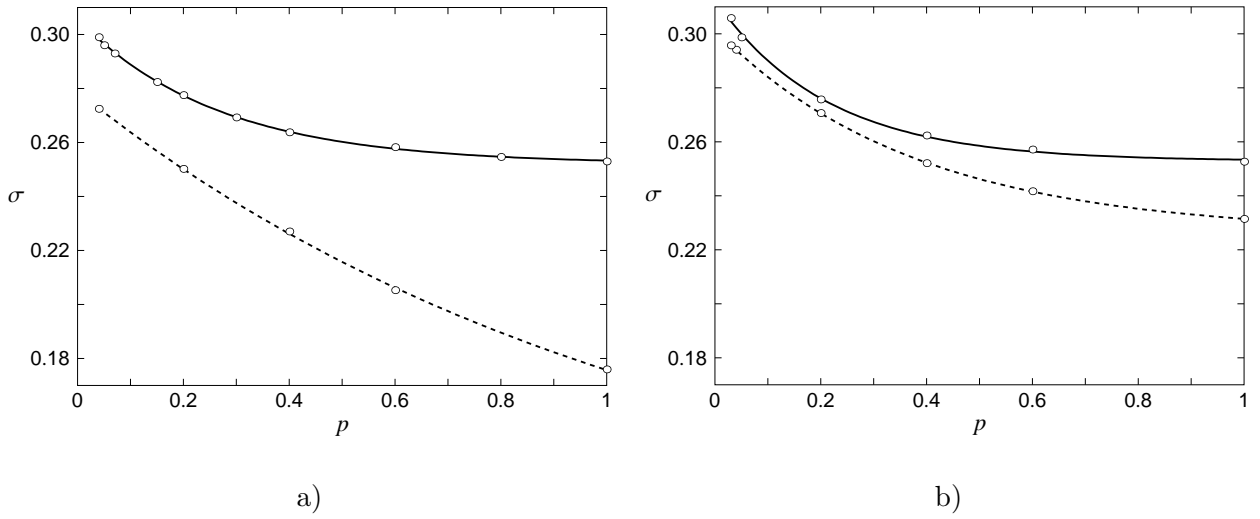
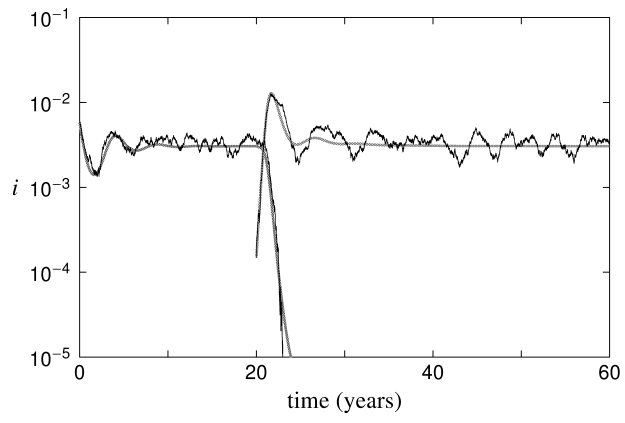
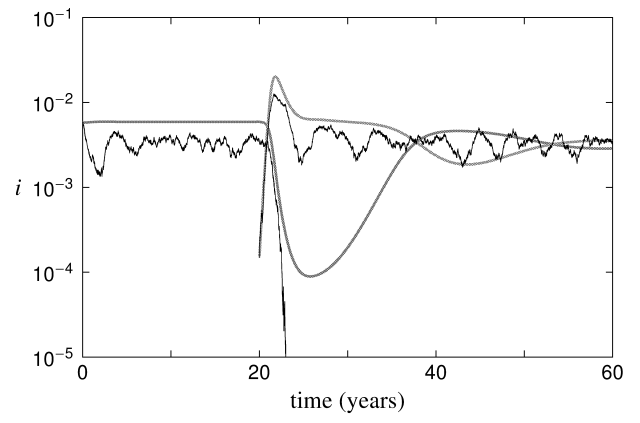


FIG. 6:



a)



b)

FIG. 7: